On reliability ~~design and code calibration~~ assessment of wind turbine blade bearings under extreme wind conditions

Ashkan Rezaei[1] and Amir Rasekhi Nejad[1]

[1]Department of Marine Technology, Norwegian University of Science and Technology (NTNU), NO-7491, Trondheim, Norway

Correspondence: ashkan rezaei (ashkan.rezaei@ntnu.no)

Abstract. This study presents ~~the reliability analysis of the blade bearing in the~~ a static-overload reliability assessment of a double-row, four-point contact ball blade bearing under ultimate limit state conditions. The National Renewable Energy Laboratory 5 MW reference wind turbine is selected for the study, and ~~the~~ a Monte Carlo simulation is used ~~for the reliability analysis and estimation of~~ to assess static-overload reliability and estimate the probability of failure. The ~~uncertainty~~ sensitivity of the probability of failure to uncertainties in turbulence intensity~~as well as materials are considered in the reliability analysis. A sensitivity analysis is carried out to evaluate the effect of bearing dimension variation. It is observed that conformity and ball diameter have the most sensitivity in the dimension aspect of reliability. IEC standards, as well as wind conditions in different wind~~ , material properties, and bearing dimensions is evaluated. Within the bounds examined, the blade bearing conformity has the largest effect on the probability of failure, and ball diameter is next. The probability of damage for case-study wind sites around the world ~~, are studied,~~ is assessed, and it is ~~shown~~ observed that the probability of failure ~~in blade bearing~~ is higher in ~~most of the wind sites than in sites with IEC standard wind~~ some cases than for wind conditions described by IEC 61400-1.

1 Introduction

Demand for wind turbines will grow ~~drastically~~ significantly over the next decade, and wind turbines are one of the main keys to meeting the IEA Net Zero Emissions by 2050, as stated in ~~IEA (2023)~~(IEA, 2023). The efficient operation of these turbines depends on various components, with blade bearings, also named pitch bearings, being a critical element. Blade bearings facilitate the smooth rotation of the turbine blades, allowing them to capture the kinetic energy of the wind at different wind speeds ~~while the loads in the turbinedon't increase~~without significantly increasing the structural loads on the turbine. Blade bearings serve as the connection point between the ~~rotor~~ blades and the hub, allowing the blades to rotate around ~~the hub. Pitch bearing assembly costs around~~ their axis. Although the entire pitch system assembly costs less than one percent of the wind turbine ~~Stehly et al. (2024); however, changing the broken~~ (Stehly et al., 2024), changing a blade bearing is costly ~~.~~ due to the need to lower the blade with a large crane. The cost of replacement with a crane can reach up to $350,000 per week (Mishnaevsky Jr and Thomsen, 2020).

A common and distinguishing feature of the blade bearings is that they involve a rather slow oscillatory motion (Harris et al., 2009) . This movement pattern differs from that of bearings in most other industrial applications, where bearings usually rotate

continuously (Menck et al., 2020). Unlike most oscillating bearings, blade bearings perform stochastic oscillations rather than constant amplitudes back and forth (Stammler et al., 2024). They oscillate through only a few degrees, up to 20° (Keller and Guo, 2022) during normal power operation, depending on wind conditions and turbine sizes, and up to 90° in emergency feathering, rather than completing full revolutions. The limited rolling distance, long dwell periods at fixed pitch angles, and frequent load reversals with high axial offsets concentrate stress cycles within a small contact zone on the raceways. Blade bearing failure consists of different ~~failure~~ damage modes, including rolling contact fatigue, core crushing, edge loading, ring fracture, rotational wear, fretting, ~~and~~ false brinelling (Andreasen et al., 2022)~~. According to standards and guidelines, it is necessary to perform the calculation of the~~ , and cage damage. Because these modes initiate in the same high-stress regions, the static-overload reliability analysis developed here directly addresses the most critical damage mechanisms for oscillating blade bearings. As part of the design and certification process, the static safety factor of the blade bearing under the ultimate limit state (ULS) ~~of bearings employing the static safety factor mentioned in ?DNV-ST-0437 (2016); Harris et al. (2009); Germanischer Lloyd (2010)~~ must be assessed, as mentioned in (IEC 61400-1, 2019; DNV-ST-0437, 2016; Harris et al., 2009; Germanischer Lloyd, 2010; Stammler et a
.

~~There are numerous studies on the fatigue of the bearings; however, the studies about the blade bearing are not many~~Several studies have analyzed blade bearings. Among them, ~~Menck et al. (2020)~~ (Menck et al., 2020) studied different lifetime calculation methods from the standards and guidelines and compared them to each other, highlighting differences in the methods and their results, and (Schwack et al., 2016) compared different fatigue lifetime calculation methods and showed huge differences in the calculated fatigue lifetime for different approaches. There are not many studies analyzing the static safety factor in blade bearings. ~~Keller and Guo (2022)~~ (Keller and Guo, 2022) studied the static load rating and safety factor of the blade bearing of a 1.5 MW wind turbine. They compared the ~~ISO 76 (2006)~~ (ISO 76, 2006) methodology with the National Renewable Energy Laboratory's (NREL's) pitch and yaw bearing design guideline (DG03) ~~Harris et al. (2009)~~ (Harris et al., 2009) and concluded that the DG03 methodology is the same as the ~~ISO 76 (2006)~~ (ISO 76, 2006) recommendation for applications subjected to shock loads. ~~Rezaei et al. (2023)~~ (Rezaei et al., 2023) studied the blade bearing of the 5 MW NREL reference wind turbine and ~~shows the importance of seed number in the turbulence wind model at bearing's life~~assessed the variation in blade bearing fatigue with shear power law exponent, turbulence intensity, and even resulting from each individual turbulent wind time series. In another work ~~Rezaei and Nejad (2023), the~~ (Rezaei and Nejad, 2023), the fatigue life of the blade bearing is compared in different wind sites and compared with IEC-designed blade bearings. ~~It is shown that the~~ The results show that fatigue life at some wind sites ~~would be lower; however, the average wind speed is far below the ? categories~~is lower, even though their average wind speeds fall below the (IEC 61400-1, 2019) category thresholds.

Even though it was shown that the results of wind sites are not the same as those of IECs, it is not clear how reliable the results are as the wind is a stochastic phenomenon. ~~Furthermore, blade bearing reliability is not studied thoroughly, and it is not clear what level of reliability one can obtain with the current design process.~~ (Haus et al.) from 55+ GW of wind plant data show that blade bearings installed pre-2016 perform fairly well, only reaching a 10% replacement rate in 15 years. However, blade bearings installed post-2016 on larger wind turbines are projected to have a 10% replacement rate in only 7.5 years. It is necessary to understand the level of reliability of any components, as it is standardized ~~in ISO 2394 (2015), ISO 19902 (2020), and ISO 19904-1 (2019) in the offshore industry. The~~ as follows:

- (IEC 61400-1, 2019) provides the reliability format (partial factors, consequence classes) for land-based wind-turbine components
- For offshore support structures, the reliability framework remains that of the ISO 19900 series—particularly (ISO 19902, 2020) (fixed steel) and (ISO 19904-1, 2019) (floating concrete)—as normatively referenced by (IEC 61400-3-1, 2019) (fixed-bottom) and (IEC 61400-3-2, 2019)(floating)
- (IEC 61400-8, 2024) gives detailed requirements for the structural components inside and around the nacelle and hub and guidance on how to account for site-specific external conditions.
- The standards didn't set reliability targets for machinery components in wind turbines.

The standards didn't set reliability targets for machinery components. The current paper studies the reliability of the blade bearing at ULS, with a deeper focus on the effect of the wind. Bearing static ~~failure~~ damage is considered a criterion for the ultimate limit state. ~~ISO 76 (2006) stated~~ (ISO 76, 2006) states that experience shows that a total permanent deformation of ~~0,0001 of the rolling element~~ 0.0001 of the ball diameter at the ~~center of the~~ most heavily loaded ~~rolling element/raceway contact can be tolerated in most bearing applications~~ contact without the subsequent ~~bearing~~ operation being impaired. ~~The bearing static failure corresponds to such a permanent deformation~~In the present study, we treat contact stresses that reach this deformation limit as attaining the ultimate limit state, i.e., stresses approaching the ISO 76 threshold are assumed to represent the onset of static failure and therefore increase the probability of bearing failure. This permanent deformation can cause ~~possibly~~ stress concentrations of considerable magnitude and the formation of cavities in the raceways. These indentations, together with conditions of marginal lubrication, can also lead to surface-initiated fatigue ~~failure Harris and Kotzalas (2006).~~ damage (Harris and Kotzalas, 2006). Although some research showed that the slewing bearing can tolerate higher total permanent deformation while no core crushing occurred, as stated in (Stammler et al., 2024), those results might be correct for a certain range of bearings with specific material and heat treatment, as stated in work by (Lai et al., 2009). The current work uses the value of 0.0001 of the rolling element diameter; however, there is a possibility that the core crushing damage does not occur in some bearings. Moreover, a sensitivity analysis on the effect of the bearing's main parameter on the probability of static failure of the blade bearing was performed.

2 Case study: wind turbine and wind sites

2.1 Reference wind turbine

Load calculations were carried out using the NREL 5MW reference wind turbine by ~~Jonkman et al. (2009)~~(Jonkman et al., 2009). It is an offshore wind turbine, designed for wind class IEC IB. The turbine properties are displayed in Table 1.

Table 1. 5 MW NREL reference wind turbine specification ~~Jonkman et al. (2009)~~(Jonkman et al., 2009)

Wind Turbine	NREL 5 MW Reference Wind Turbine
Rating	5 MW
Rotor Diameter	126 m
Hub Height	90 m
Drivetrain	High-speed, multiple-stage gearbox
Minimum and Rated Rotor Speed	6.9 rpm, 12.1 rpm
Cut-In, Rated, Cut-Out Wind Speed	3 m/s, 11.4 m/s, 25 m/s
Overhang, Shaft Tilt, Precone	5 m, 5°, 2.5°
Rotor Mass	110,000 kg
Nacelle Mass	240,000 kg
Tower Mass	347,460 kg

2.2 Blade bearing

The ~~blade bearing~~ blade-bearing model is considered from work by ~~Rezaei et al. (2023)~~(Rezaei et al., 2023). The bearing is a double-row, four-point contact ball bearing with a total of 250 balls. The general specification of the bearing is presented in Table 2. The details of the bearing specifications and dimensions can be accessed at ~~Rezaei et al. (2023)~~(Rezaei et al., 2023).

Table 2. Blade bearing main dimensions

Parameter	Value	Description
D_{pw}	3558	Bearing pitch diameter (mm)
D	75	Ball diameter (mm)
α	45	Initial contact angle (°)
Z	125	Number of balls per row
i	2	Number of rows
f_i	0.53	Inner raceway groove radius/D
f_o	0.53	Outer raceway groove radius/D

2.3 Wind sites

The wind regimes consist of IEC-category wind fields and wind sites. IEC-category wind fields consist of three wind speed classes: I, II, and III. Each wind speed class has four subclasses of A+, A, B, and C based on turbulence intensity. The basic parameters of the wind turbine classes are presented in Table 3 ~~(?)~~(IEC 61400-1, 2019). In the table V_{ave} is the annual wind speed, V_{ref} is the reference wind speed ~~average~~ averaged over 10 minutes, and I_{ref} is the reference value of the turbulence intensity.

Table 3. Basic parameters for IEC-category wind turbine ~~?~~(IEC 61400-1, 2019)

Wind turbine class	I	II	III
V_{ave} (m/s)	10	8.5	7.5
V_{ref} (m/s)	50	42.5	37.5
A+, I_{ref}		0.18	
A, I_{ref}		0.16	
B, I_{ref}		0.14	
C, I_{ref}		0.12	

The wind sites include 13 in Iran ~~SATBA (2022), Pakistan World Bank Group (2023b), Vietnam GIZ (2023), Ethiopia World Bank Group (2023a), Denmark Ørsted (2022)~~(SATBA, 2022), Pakistan (World Bank Group, 2023b), Vietnam (GIZ, 2023), Ethiopia (World Bank Group, 2023a), Denmark (Ørsted, 2022), and the United States of America ~~Jager and Andreas (1996)~~ (Jager and Andreas, 1996). The wind data includes the mean and standard deviation of 10-min wind speed. In order to account for the wind's seasonal effect, data needs to cover an entire year. ~~Nominated~~ The nominated wind sites cover a whole year's measurements. More information on the wind sites is presented at work by ~~Rezaei and Nejad (2023)~~(Rezaei and Nejad, 2023).

3 Methodology

3.1 Structural reliability

The study of structural reliability is concerned with calculating and predicting the probability of limit state violation for an engineered system at any stage during its life as defined by ~~Melchers and Beck (2018). Nejad (2018)~~ (Melchers and Beck, 2018). (Nejad, 2018) named the main aim of the structural reliability as an estimation of the failure probability by taking into account explicitly uncertainties of the load, load effect, and resistance.

Ultimate limit state reliability in the current work is based on a static safety factor. The procedure for the ultimate limit state calculated in this paper is illustrated in Fig. 1. In the next section, the procedure for each step is presented.

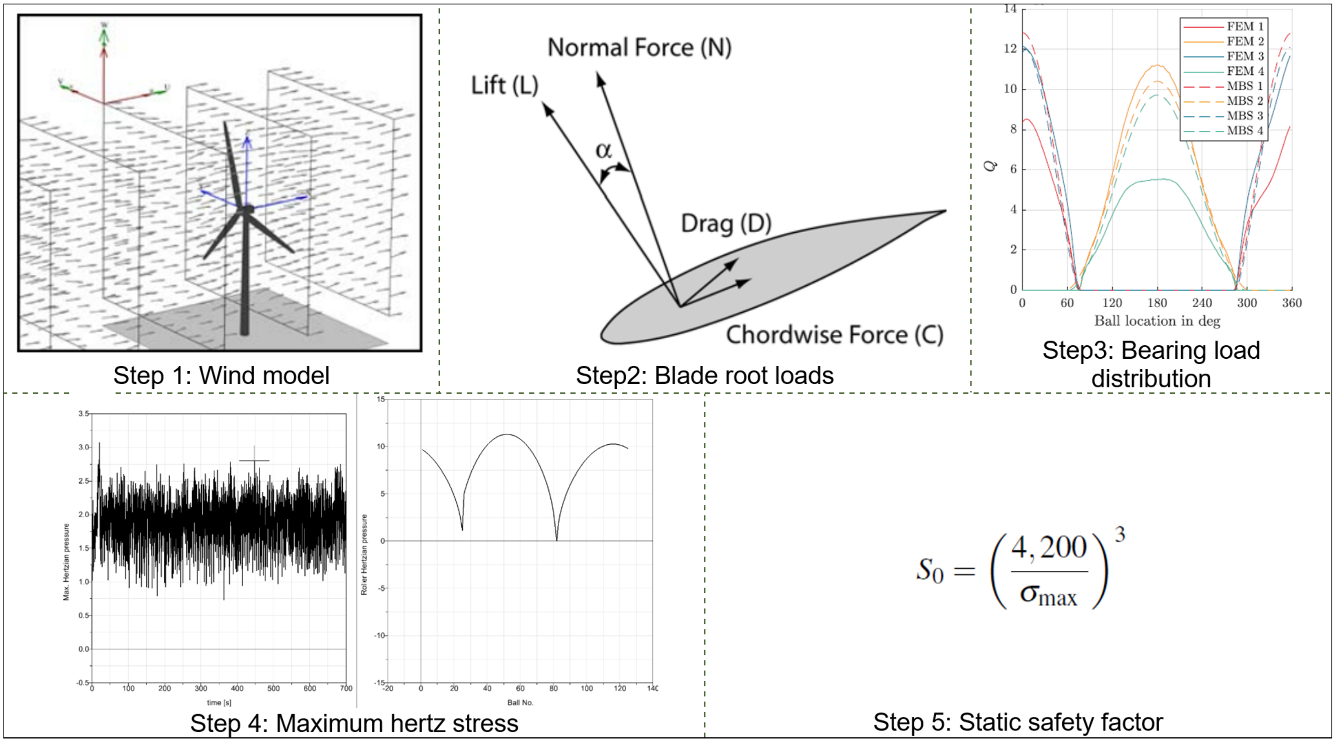

Figure 1. Illustration of the procedure ~~that~~ used to calculate the static safety factor~~is calculated~~

3.2 Safety factor and failure function

A safety factor is a measure used in engineering and design to provide a margin of safety for structures, materials, or systems under expected loads or conditions. It accounts for uncertainties in the design process, such as variations in material properties, manufacturing tolerances, unexpected loads, and potential degradation over time. In this study, the formula that is used for the failure function has the same ~~formation~~ form as the static calculation function and static safety factors.

~~The safety factor, according to ISO 76 (2006), is a ratio between the basic static load rating and the static equivalent load, giving a margin of safety against inadmissible permanent deformation on rolling elements and raceways, and is defined as~~

$$S_0 = \frac{C_{0a}}{P_{0a}}$$

~~where C_{0a} is the basic static axial load rating~~

$$C_{0a} = f_{0a} i Z D^2 sin\alpha$$

~~and P_{0a} the static equivalent axial load.~~

$$P_{0a} = 2.3 F_r tan\alpha + F_a$$

~~f_{0a} is a geometric factor, calculated from Table 1 in ISO 76 (2006). F_a in P_{0a} includes both direct axial force and axial force due to the bending moment on the bearing. Another approach is to consider~~ For the reliability model, the static limit state is formulated with the Hertzian contact-stress criterion. The approach considers that bearing static ~~failure~~ damage occurs when the maximum Hertz contact stress exceeds the allowable Hertz contact stress. In this regard, the static safety factor (~~SF~~S_0) is the ratio of the allowable ball load to the actual ball load ~~Harris et al. (2009)~~(Harris et al., 2009). The DG03 uses a comparison of the maximum contact stress, ~~σ_{max}~~$\sigma_{\max}$, in the limit load condition to the maximum allowable stress of 4,200 ~~MPa~~ megapascals to define the static safety factor as ~~Harris et al. (2009) and Stammler et al. (2024)~~ (Harris et al., 2009) and (Stammler et al., 2024)

$$S_0 = (\frac{4200}{\sigma_{max}} \frac{4200}{\sigma_{\max}})^3 \tag{1}$$

where the maximum contact stress, σ_{max}, is also expressed in megapascals ~~calculated as~~ (MPa) calculated as

$$\sigma_{max} = \frac{1.5 Q_{max}}{\pi ab} \frac{1.5 Q_{\max}}{\pi ab} \tag{2}$$

and the static safety factor can be rewritten as

$$S_0 = \left(\frac{\frac{4200\pi ab}{1.5}}{Q_{max}} \frac{\frac{4200\pi ab}{1.5}}{Q_{\max}} \right)^3 \tag{3}$$

In equation 2, πab is the contact area, which is an ellipse having semi-major axis ~~a~~ a and semi-minor axis ~~b, and Q_{max}~~ b, and Q_{max} is the maximum ball force. The maximum ball load is calculated from (Stammler et al., 2024)

$$Q_{max\,\mathrm{max}} = 0.55\left(\frac{2F_r}{Zcos\alpha}\frac{2F_r}{Z\,\cos\alpha} + \frac{F_a}{Zsin\alpha}\frac{F_a}{Z\,\sin\alpha} + \frac{4.4M}{D_{pw}Zsin\alpha}\frac{4.4M}{D_{\mathrm{pw}}\,Z\,\sin\alpha}\right) \tag{4}$$

where F_r, F_a, and M denote the applied radial, axial, and moment loads, respectively. ~~D_{pw} denotes the pitch diameter of the bearing. z is the number of balls and α is the contact angle.~~

In Equation 3, the numerator and denominator are named R and S, respectively. a and b in the R are functions of the applied maximum ball load Q_{max}; therefore, R is implicitly a function of S. The failure function, g_x, is defined below, where x ~~is~~ are random variables and n is the static safety ratio.

$$g_x(R,S) = (\frac{R}{S})^3 \leq n \tag{5}$$

The static safety ratio, n, determines the boundary of the ~~failure~~damage. If the failure function value is equal to or ~~greater~~ smaller than the static safety ratio, the bearing is ~~safe~~in a failure state; otherwise, the bearing is in a ~~failure~~ safe state. In a work by ~~Keller and Guo (2022)~~(Keller and Guo, 2022), it is recommended that the static safety ratio be greater than 1.5; however, ~~Stammler et al. (2024)~~ (Stammler et al., 2024) noted that it seems reasonable to refer to the limit of 1 such as ~~?~~ (IEC 61400-1, 2019). In order to compute the actual reliability and allow for comparisons, the static factor ratio equal to 1 is considered. Consequently, g_x will become

$$g_x(R,S) = (\frac{R}{S})^3 \leq 1 \tag{6}$$

~~The failure function can be written as~~

$$g_x(R,S) = R^3 - S^3 \leq 0$$

~~and~~

$$g_x(R,S) = (R-S)(R^2 + RS + S^2) \leq 0$$

~~In order to make the failure function negative, one of the two terms in Equation **??** should be negative. The second parenthesis in Equation **??** is always positive, so the first term $(R-S)$ should be negative to make the failure function negative. Therefore, the failure function would be~~ Taking the cube root of Equation 6 yields the failure function directly as

$$g_x(R,S) = R - S \leq 0 \tag{7}$$

The annual probability of failure, P_f, is then obtained from

$$P_f = P(g_x(R,S) \leq 0) = P(R - S \leq 0) \tag{8}$$

To ~~find~~ compute P_f ~~different methods of the first-~~, different methods can be used, including first-order and second-order reliability methods (FORM and SORM), ~~and Monte Carlo can be used Ditlevsen and Madsen (2007).~~ as well as the Monte Carlo method (Ditlevsen and Madsen, 2007). In this study, the Monte Carlo simulation ~~has been used in this paper~~method is employed to estimate the probability of failure. By the Monte Carlo simulation method, a suitably large sample of typical load configurations is simulated from the probabilistic action model. This load configuration sample gives a corresponding sample of load effects at different points of the bearing, and from this sample, the probability distributions of the load effects can be estimated. By using these probability distributions, extreme value studies can next be made. In this sense, the probabilistic model uses typical load configurations in its solution procedure and not difficult choices of “extreme" load configurations as they are used in the deterministic model ~~Ditlevsen and Madsen (2007)~~(Ditlevsen and Madsen, 2007).

The randomness of the failure function arises from different aspects. Uncertainties in material, forces, and models are some of the main ones. These ~~randomnesses~~ sources of randomness can appear in the R ~~or S or both, which represent the resistance and stress due to external loads in the bearing, respectively~~representation of the load-capacity term and S the representation of the applied maximum ball load. The randomness in ~~resistance and stress~~ R and S in the current work originated from uncertainty in the materials, dimensions, wind turbulence intensity, and simulation model in ball forces. ~~In Fig. 2~~ Figure 2 presents a systematic approach for the ~~reliability analysis~~ static overload reliability assessment of a blade bearing~~is presented~~.

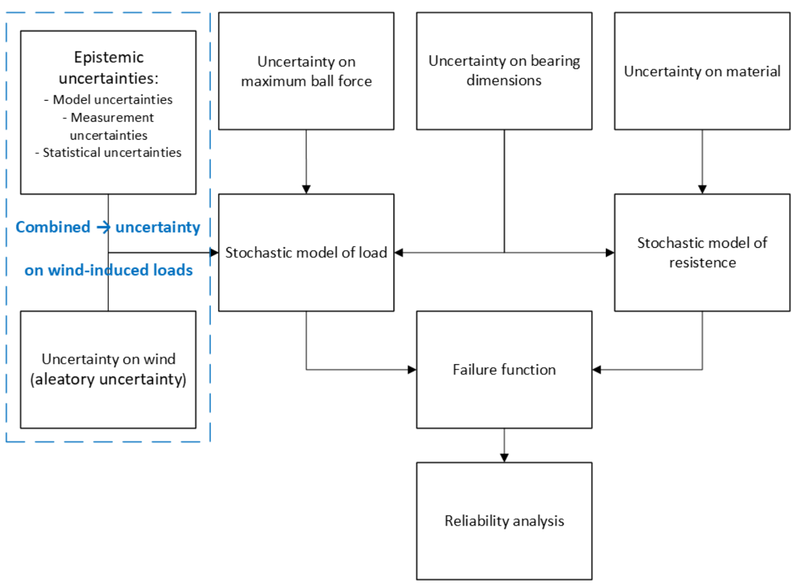

Figure 2. Flowchart of reliability ~~analysis~~ assessment in a blade bearing for ultimate limit state

The dashed box represents uncertainty on loads that have distinct uncertainty sources -(i) external wind variability and (ii) Epistemic uncertainty arises from model, measurement, and stochastic uncertainties, which are sampled separately and then combined to generate the stochastic wind-induced loads. The uncertainties of the measurement and statistics are not considered in this study. Uncertainty in material leads to uncertainty in resistance, while uncertainty in dimension leads to both uncertainty in stress and resistance. The formula for resistance extracted from Equation 9 with consideration of uncertainty in material and dimension is presented below,

$$R = \left(\frac{4200\chi_m \pi a(\chi_d) b(\chi_d)}{1.5}\right) \tag{9}$$

where χ_m and χ_d are ~~uncertainty~~ uncertainties in material and dimension, respectively. Uncertainty in dimension has an effect on the ~~dimension~~ dimensions of the contact area, a and b. It should be noted that a and b are, in addition to the uncertainty in dimension, functions of uncertainty in the loads and the maximum ball forces ~~.~~ $Q_{\max}$. In every Monte-Carlo realization, therefore, $Q_{\max}$ is computed first, then evaluated a, b, and finally R, ensuring that the dependency R(S) is fully captured. The formula that represents S, presented below~~,~~.

$$S = \left(Q_{\underline{max}\,\mathrm{max}}\chi_f\right) \tag{10}$$

where χ_f is uncertainty in maximum ball force. ~~Q_{max}~~ $Q_{\max}$ contains external loads and bearing dimensions, which in fact are uncertain parameters. Therefore, in its nature, it consists of uncertainty.

The probability of failure including all uncertainties will then be

$$P_f = P(\left(\frac{4200\chi_m \pi a(\chi_d) b(\chi_d)}{1.5}\right) - \left(Q_{\underline{max}\,\mathrm{max}}\chi_f\right) \leq 0) \tag{11}$$

3.2.1 Uncertainty in material

The strength of bearings is not a deterministic value. ~~ISO 76 (2006)~~ (ISO 76, 2006) recommends a Hertz contact stress of 4200 MPa for ball bearings, which is equivalent to a total permanent deformation of 0.0001 of the rolling element diameter. Assessing the uncertainty of the material's strength requires extensive testing. ~~Shimizu et al. (2010)~~ (Shimizu et al., 2010) presented the mechanical properties of the AISI 52100 bearing steel. They showed that tensile strength and Rockwell C hardness have a normal distribution with a standard deviation of 5.7% and 1.1%, respectively. ~~Lewis et al. (2015)~~ (Lai et al., 2009) presented a model for plastic indentation, and they tested it on 42CrMo4 steel. Their model predicted that the contact pressure for causing plastic indentation of $10^{-4}D$ in the through-hard raceway is 4260 MPa, as well as good validation results. In the extended work, (Lai, 2011) predicted the contact pressure to be 4270 MPa. (Lewis et al., 2015) assessed 9 different sources, including 7 bearing manufacturers, and allowable peak Hertzian pressures of 4270 MPa and 3962 MPa for SAE 52100 steel and AISI 440C steel, respectively, based on the mean minimum hardness. ~~Wang and Zhang (2022)~~ (Wang and Zhang, 2022) performed a reliability analysis on an angular contact ball bearing. They considered allowable yield stress as a strength parameter with a 5% standard deviation. In another work, density and ~~module~~ modulus of elasticity in work by ~~Cheng et al. (2020) is~~ (Cheng et al., 2020) are considered a normal distribution with a 5% standard deviation. In their sensitivity analysis, they concluded that the material has the highest reliability sensitivity. ~~The~~ (Imdad et al., 2024) studied 42CrMo4 steel that was submitted to different heat treatments and hardness levels. The hardness level in different heat treatments has a deviation between 2% and 6.5%. The current work considered a normal distribution with a standard deviation of 5.7% for the uncertainty of material, χ_m.

3.2.2 Uncertainty in dimensions

Blade bearing dimensions affect the loads and resistance in the failure function. ~~Wang and Zhang (2022)~~ (Wang and Zhang, 2022) performed a sensitivity analysis on four parameters of the bearing, including ball pitch diameter, ball diameter, and inner and outer raceway groove curvature with normal distributions and 0.5% standard deviations. They concluded that, regarding the bearing geometry, the ball diameter has the highest effect on reliability to prevent plastic deformation. ~~Cheng et al. (2020) in sensitivity analysis on~~ In (Cheng et al., 2020)'s sensitivity analysis of an angular contact ball bearing, the free contact angle ~~, and~~ and the inner and outer ~~raceways were considered random parametersapart from~~ raceway curvatures were treated as random parameters, along with the ball diameter and groove curvatures. All of their random parameters had 0.5% standard deviations. In a reliability and sensitivity analysis of spherical roller bearings, ~~Wang et al. (2020)~~ (Wang et al., 2020) considered 4%, 2.2%, and 0.5% standard deviation for ~~ball~~ roller diameter, pitch diameter, and radial clearance, respectively. The effect of dimensions on the reliability of the bearing is presented in the ~~sensetivity~~ sensitivity analysis section. It should be noted that each dimension was analyzed independently by the relevant distribution.

3.2.3 Uncertainty in loads

~~Wang and Zhang (2022)~~(Wang and Zhang, 2022), in their work, considered normal distributions with a 5% standard deviation for axial and radial forces. The same consideration at work by ~~Cheng et al. (2020)~~ (Cheng et al., 2020) has been seen. In contrast, ~~Wang et al. (2020)~~ (Wang et al., 2020) considered a standard deviation of 2.5% for the radial load.

The uncertainty of the load at the blade bearing originates mainly from ~~the turbulence of~~ turbulence acting on the wind turbine, and the turbulence has a great contribution to both the safety factor and the fatigue life of the blade bearing, as shown in the work by ~~Rezaei et al. (2023)~~(Rezaei et al., 2023). Different realizations of the turbulence~~intensity were considered with different random seed numbers. Different seed numbers~~ , called "seed number," produce a Gaussian distribution of TI in the longitudinal wind component ~~, due to the spatial coherence . In other words, seed numbers are used to create random phases (one per frequency per grid point per wind component) for the velocity time series in the turbulence wind model Jonkman (2009).~~ due to spatial coherence (Jonkman, 2009).

Each simulation with a specific seed number leads to a time series of distributions of the loads in the balls, while the extreme ball load can be obtained from these series. Different random seed number simulations result in a series of extreme ball loads in the blade bearing while the turbulence intensity is constant. These extreme loads form a probability distribution function. It is important to assign a proper probability distribution function to these extreme loads.

In this study, the following probability distribution functions ~~of generalized extreme value~~were considered: the Generalized Extreme Value, Gamma, ~~inverse~~ Inverse Gaussian, Kernel, ~~lognormal~~Lognormal, Nakagami, Rician, and Weibull ~~were considered~~distributio In Table 4, the probability density function (PDF) of the nominated distribution function is presented, where x is a random variable. More information on the equations and parameter definitions of generalized extreme value, Gamma, Kernel, and Weibull is referred to in ~~Shi et al. (2021)~~(Shi et al., 2021). The parameters of inverse Gaussian, lognormal, and Nakagami are referred to in ~~Alavi et al. (2016)~~(Alavi et al., 2016). Rician parameters are referred to in ~~Yu et al. (2019)~~(Yu et al., 2019).

Table 4. PDFs of nominated distribution function ~~Alavi et al. (2016); Shi et al. (2021); Yu et al. (2019)~~ (Alavi et al., 2016; Shi et al., 2021; Yu et al., 2019)

Distribution function	PDF
Generalized Extreme Value (GEV)	$f(x) = \frac{1}{\alpha}[1 - \frac{k}{\alpha}(x-\mu)]^{\frac{1}{k}-1} - e^{-[1-\frac{k}{\alpha}(x-\mu)]^{\frac{1}{k}}}$
Gamma (Gam)	$f(x) = \frac{\alpha^k}{\Gamma(k)} x^{k-1} e^{-\alpha x}$
Inverse Gaussian (IG)	$f(x) = \sqrt{\frac{\lambda}{2\pi x^3}} e^{-\frac{\lambda}{2\mu^2 x}(x-\mu^2)}$
Kernel (Ker)	$f(\alpha) = \frac{1}{nh}\sum_{i=1}^{n} K(\alpha), \quad \alpha = \frac{x-x_i}{h}$
Lognormal (LN)	$f(x) = \frac{1}{x\sigma\sqrt{2\pi}} e^{-\frac{1}{2}[\frac{ln(x)-\mu}{\sigma}]^2}$
Nakagami (Nak)	$f(x) = \frac{2m^m}{\Gamma(m)\Omega^m} x^{2m-1} e^{-\frac{m}{\Omega}x^2}$
Rician (Ric)	$f(x) = \frac{x}{a^2} e^{-\frac{x^2+b^2}{2a^2}} I_0(\frac{bx}{a^2})$
Weibull (Wbl)	$f(x) = \frac{k}{\alpha}(\frac{x}{\alpha})^{k-1} e^{-(\frac{x}{\alpha})^k}$

In this study, the parameters were calculated by the maximum likelihood estimator ~~Bain and Antle (1967)~~ (Bain and Antle, 1967) using MATLAB software, and to assess the performance and goodness-of-fit (GoF) of the distribution functions, the coefficient of efficiency method (CE) has been applied. CE is intended to range from zero to one, but negative scores are also permitted. The maximum positive score of one represents a perfect model; a value of zero indicates that the model is no better than a one-parameter "no knowledge" model in which the forecast is the mean of the observed series at all time steps; negative scores are unbounded; and a negative value indicates that the model is performing worse than a "no knowledge" model according to ~~Dawson et al. (2007)~~(Dawson et al., 2007). The CE indicator is one minus the ratio of the sum square error to the statistical variance of the observed dataset about the mean of the observed dataset.

$$CE = 1 - \frac{\sum(Q_i - \hat{Q}_i)^2}{\sum(Q_i - \bar{Q})^2} \tag{12}$$

Q_i is observed data at level i, $\hat{Q}_i$ is estimated data at level i, and $\bar{Q}$ is the mean of observed data.

Different seed numbers were studied to create a distribution function. According to ~~?~~(IEC 61400-1, 2019), in ultimate strength analysis, 15 different simulations are necessary for each wind speed from $(V_r - 2m/s)$ to cut-out, and six simulations are necessary for each wind speed below $(V_r - 2m/s)$. However, for generating coherent turbulent structures, using more than 30 different random seeds for a specific set of boundary conditions is recommended by ~~Jonkman (2009)~~(Jonkman, 2009) . This study covers a wide range of seed numbers. The generalized extreme value ~~is considered for~~ distribution is selected to model the maximum load distribution~~function~~. The reason behind is presented in the results section.

3.2.4 Uncertainty in the maximum ball force

The uncertainty in the maximum ball forces arises from the distribution of the forces inside bearings. The flexibility of the bearings and connecting components, hub and blade, can affect the load distributions inside the bearing, as ~~were~~ was shown in works by ~~Menck et al. (2020) and Rezaei et al. (2024)~~(Menck et al., 2020) and (Rezaei et al., 2024). In addition, the results of the maximum ball force equation are not necessarily conservative. It can overestimate or underestimate the actual loads ~~Stammler et al. (2024)~~(Stammler et al., 2024).

~~Menck et al. (2020)~~ (Menck et al., 2020) developed a finite element model (FEM) and calculated the bearing load distributions. Moreover, ~~Graßmann et al. (2023)~~ (Graßmann et al., 2023) validated the finite element model with extensive experimental data on the blade bearing. Furthermore, ~~Rezaei et al. (2024)~~ (Rezaei et al., 2024) compared the load distribution from the finite element model and multi-body simulations (MBS) for NREL 5MW and IWES 7.5 MW wind turbines. The average of the maximum ball force differences between MBS and FEM was 10.8%. In another work by ~~Leupold et al. (2021)~~ (Leupold et al., 2021), load distributions inside the bearing for two different conditions of finite element and multi-body simulation were studied, and the average error was 6.5%.

The maximum ball forces and load distributions in the work by ~~Rezaei et al. (2024)~~ (Rezaei et al., 2024) were recalculated with the maximum ball force equation. The differences between the maximum forces from FEM and the maximum ball equation have a mean and standard deviation of 13% and 6.5%, respectively, which is considered an uncertainty of maximum ball forces, χ_f.

The distributions and the mean and standard deviation of model uncertainties based on the above discussions are summarized in Table 5.

Table 5. Uncertainty distributions

Uncertainty	Distribution	Mean	St. dev.
χ_f	Normal	1.13	0.065
χ_m	Normal	1	0.057
χ_d	Normal	1	0.005
~~Q_{max}~~ $Q_{\max}$	GEV	Distribution depends on each wind condition	

3.3 Description of DLC

It is observed that design load case (DLC) 1.3 of IEC ~~61400~~ 61400-1, around rated wind speed, has the largest effect on the load of the blade bearings ~~Rezaei et al. (2023)~~(Rezaei et al., 2023); therefore, it is considered a nominated load case.

The DLC 1.3 contributes to an extreme turbulence model (ETM). ~~DLC covered the mean wind speed~~ The DLC covered mean wind speeds from 10 to 13 m/s with an interval of 0.5 m/s. The simulations last 700 seconds, and the results of the first hundred seconds are not considered. In all DLCs, wind shear is considered according to the sites or related standard conditions. The extreme TIs in the wind sites are presented in Table 6.

Table 6. Extreme turbulence intensity in wind sites

Wind speed (m/s)	Khaf	Mil nader	Shourjeh	Bafrajerd	Moaleman	Sujawal	ThanhHai	Aysha	Gode	Kebribeyah	Tuluguled	Flatirons	Anholt
10.5	0.3143	0.2682	0.4149	0.4825	0.2927	0.6513	0.3688	0.8773	0.2608	0.3641	0.3421	0.4517	0.2341
11	0.3412	0.3957	0.4616	0.3575	0.3109	0.171	0.5272	0.4422	0.261	0.5717	0.3427	0.4771	0.2193
11.5	0.361	0.2295	0.5302	0.3914	0.295	0.2135	0.3807	0.3493	0.2736	0.3364	0.3243	0.4953	0.2928
12	0.4366	0.1926	0.3572	0.3623	0.4885	0.166	0.5161	0.406	0.2406	0.3722	0.4477	0.3938	0.2467
12.5	0.3735	0.2587	0.3159	0.3683	0.2652	0.1659	0.3542	0.2318	0.237	0.3343	0.3629	0.4607	0.1704
13	0.3592	0.316	0.3188	0.3736	0.3125	0.1775	0.374	0.2707	0.2092	0.2537	0.1985	0.3577	0.1675

4 Results and discussion

4.1 Probability distribution function

Seed numbers from 15 to 3000 were studied in onshore wind conditions in IEC category IA. The results of the ~~fitted distribution~~ probability density function and exceedance probability of the fitted distributions for border seed numbers 15 and 3000 are depicted in Fig. ~~??.~~ 3 and Fig. 4.

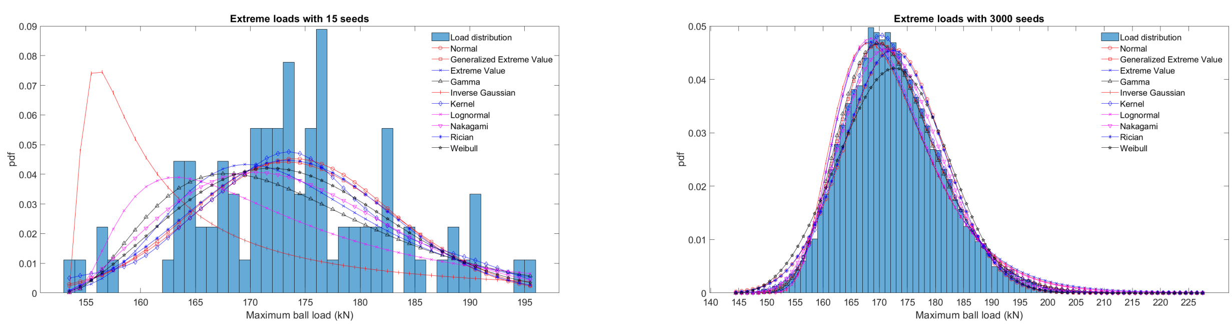

Figure 3. Annual probability density function of different distribution functions in 15 seeds (left) and 3000 seeds (right)

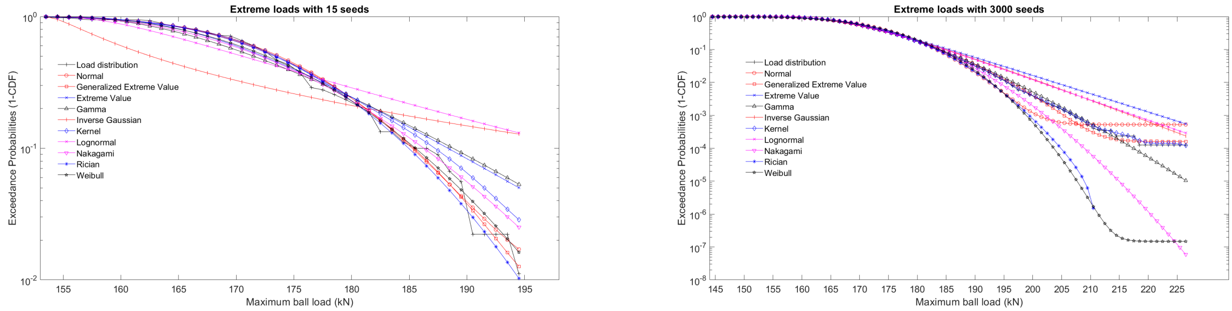

Figure 4. The exceedance probabilities of different distribution functions in 15 seeds (left) and 3000 seeds (right)

CE indicator results in different seed numbers with nominated probability distribution functions are presented in Table 7

Table 7. Coefficient of efficiencies of the nominated probability distribution functions in different seed numbers

PDF	CE														
	15	30	50	75	100	150	200	300	600	900	1200	1500	1800	2400	3000
Nor	0.464	0.677	0.793	0.753	0.871	0.872	0.944	0.942	0.961	0.961	0.972	0.971	0.977	0.977	0.977
GEV	0.461	0.672	0.858	0.807	0.921	0.914	0.974	0.972	0.982	0.982	0.993	0.994	0.994	0.995	0.996
EV	0.409	0.587	0.855	0.814	0.911	0.906	0.951	0.949	0.953	0.953	0.970	0.975	0.970	0.971	0.976
Gam	0.307	0.517	0.846	0.812	0.912	0.913	0.958	0.963	0.970	0.970	0.985	0.993	0.984	0.988	0.995
IG	-1.218	-0.685	0.614	-0.169	0.802	0.791	0.818	0.805	0.860	0.860	0.911	0.965	0.904	0.932	0.968
Ker	0.510	0.703	0.867	0.836	0.928	0.920	0.977	0.975	0.989	0.989	0.997	0.997	0.997	0.999	0.999
LN	0.023	0.262	0.767	0.691	0.865	0.883	0.899	0.921	0.927	0.927	0.949	0.977	0.946	0.957	0.978
Nak	0.392	0.613	0.852	0.822	0.913	0.909	0.969	0.966	0.978	0.978	0.990	0.990	0.992	0.993	0.994
Ric	0.459	0.667	0.834	0.791	0.888	0.881	0.953	0.948	0.965	0.965	0.977	0.974	0.981	0.980	0.979
Wbl	0.429	0.641	0.846	0.812	0.897	0.883	0.955	0.939	0.955	0.955	0.971	0.957	0.975	0.971	0.964

The results show that the kernel and generalized extreme value ~~best perform~~ distributions perform best in modeling the extreme load distribution. This dominance started with 150 seeds. The kernel estimator does not have a closed formula, and the generalized extreme value is considered a distribution for modeling the effect of seed number ~~in~~ on the distribution of extreme loads. The results also indicate that a low number of seed values cannot accurately represent the true variety of the extreme loads.

Changes in the mean of the GEV function due to the seed number are plotted in Fig. 5.

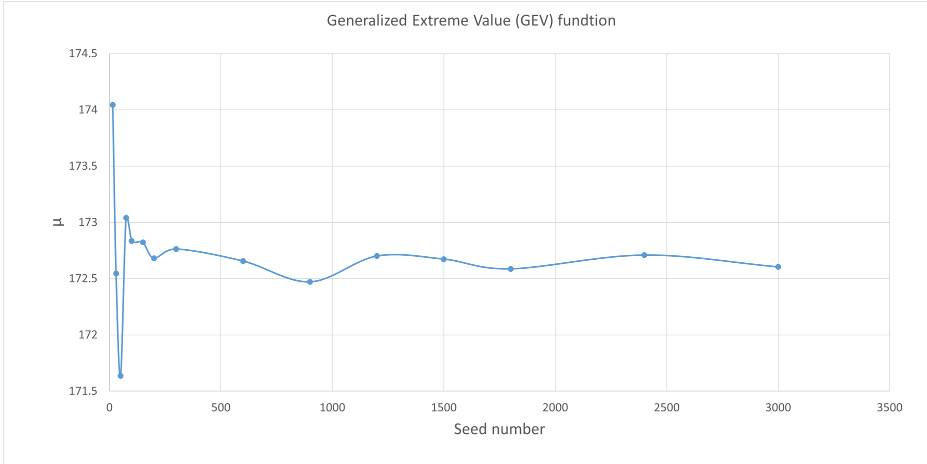

Figure 5. Changes of ~~the~~ mean of generalized extreme value distribution due to seed numbers

It is very time-consuming to consider the high number of random seeds in the simulations. In addition, changes in the GEV parameters in 300 seeds and more are less than 3%. The 300 seed number is the value that is considered for the random seed number in the rest of the results.

4.2 Sensitivity analysis

The probability of failure ~~(Pf)~~ in the bearing with variation in the ball diameter, pitch circle diameter, conformity, and contact angle is studied. The onshore wind field with a turbulence intensity grade of IA according to IEC ~~61400~~ 61400-1 is considered. 10^8 samples were considered in the simulation with the Monte Carlo method, and this process was repeated 20 times. ~~It is observed that raceway conformity has the dominant effect on blade bearing failure in ULS. Consequently, the uncertainty of the raceway conformity with normal distribution with a standard deviation of %0.5 for the uncertainty of dimension,~~ ~~χ_d, is considered.~~

4.2.1 Ball diameter

The nominal size of the ball diameter is 75 mm. ~~It~~ Although the balls are usually manufactured and sorted in a batch with fine tolerances in diameters, it is assumed that the ball diameter can change from fine to very coarse machining according to ISO 2768-1 ~~ISO 2768-1 (1989). It~~ (ISO 2768-1, 1989). In every analysis, the balls' diameters are assumed to be the same, and a range of diameters was studied. However, the extreme tolerances are not realistic; they can help to observe the trend of changes in reliability. The assumption leads to a 0.15 to 1.5 mm variation in the ball diameter. The failure probability of the bearing with different ball diameters is shown in Fig. 6a. Increasing the ball diameter increases the reliability of the bearing, which is in good agreement with the results from ~~Wang and Zhang (2022)~~ (Wang and Zhang, 2022); however, the reliability decreases more sharply in their analysis.

4.2.2 Pitch circle diameter

The nominal size of the pitch circle diameter is 3558 mm. It is assumed that the pitch circle diameter can change from medium (2 mm) to very coarse (8 mm) machining~~according to ISO 2768-1 (1989)~~, according to (ISO 2768-1, 1989). In order to observe the wider range of diameters, diameters of 3540 and 3576 mm were added to the study. The failure probability of the bearing with different pitch circle diameters is shown in Fig. 6b. The results show that the pitch circle diameter does not have a significant effect on the ~~Pf~~P_f.

4.2.3 Raceway conformity

Raceway conformity is the dimensional relationship between the radius of the raceway and the diameter of the ball. The nominal size of the conformity in the current study is 0.53. According to ~~Daidié et al. (2008)~~(Daidié et al., 2008), bearing manufacturers recommend a value between 0.510 and 0.543 for this ratio. In this study, the conformity between 0.515 and 0.545 is studied. The failure probability of the bearing with different raceway conformities is shown in Fig. 6c. The results of the ~~Pf~~ P_f show that with an increase in conformity, reliability sharply decreases. ~~Wang and Zhang (2022)~~ (Wang and Zhang, 2022) reached the same conclusion, but the decrease in reliability was not as sharp as the results presented. ~~Wang et al. (2016) got the same results in~~ (Wang et al., 2016) obtained similar results regarding the maximum Hertzian contact stress in their ~~research for~~ study on angular contact ball bearings. In order to understand how much the manufacturing of the ball and raceway can affect the reliability of the bearing, it is assumed that the ball and raceways have a fine degree of manufacturing according to ~~ISO 2768-1 (1989)~~(ISO 2768-1, 1989), where in our study the tolerance would be 0.15 mm and the extreme values for conformity would be 0.527 and 0.533. The extreme values for the raceway conformity by this assumption are shown with vertical lines in Fig. 6c. It is observed that raceway conformity has the dominant effect on blade bearing damage in ULS. Consequently, the uncertainty of the raceway conformity with normal distribution with a standard deviation of 0.5% for the uncertainty of dimension, χ_d, is considered.

4.2.4 Contact angle

The nominal size of the initial contact angle is 45 degrees. The ~~contact angle~~ initial contact angle in this study referred to the nominal contact angle, which is in a load-free condition. The contact angle from 25 °to 65 °is studied. The failure probability of the bearing with different contact angles is shown in Fig. 6d.

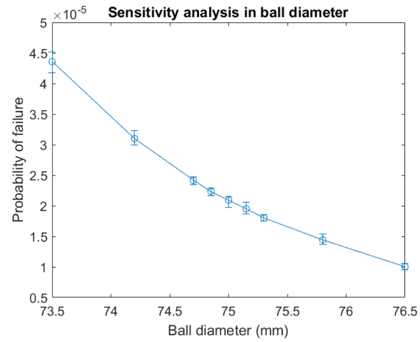

(a)

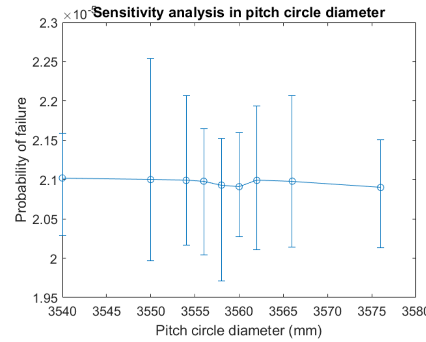

(b)

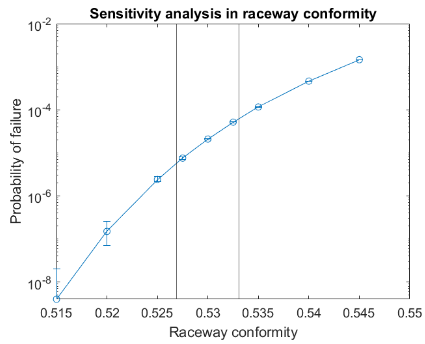

(c)

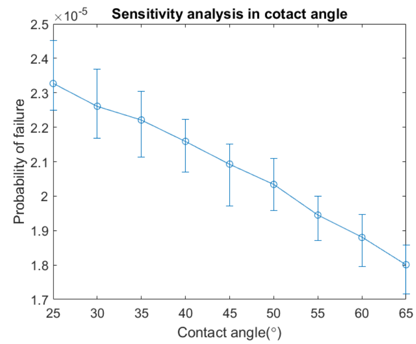

(d)

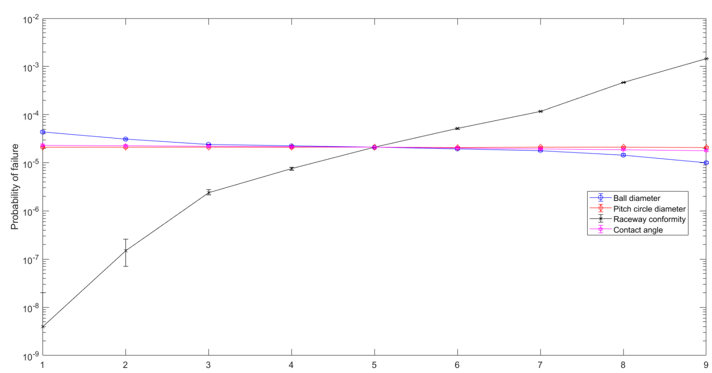

(e)

Figure 6. P_f with different (a) ball diameter, (b) pitch circle diameter, (c) raceway conformity, (d) contact angle, and (e) combining a to d

The results show that the probability of failure decreases ~~by increasing~~ as the contact angle ~~. Cheng et al. (2020)~~ increases. (Cheng et al., 2020) got the same results in the shear stress in their research for angular contact ball bearings.

~~The probability of failure with different (a) ball diameter, (b) pitch circle diameter, (c) raceway conformity, (d) contact angle~~

4.3 IEC wind conditions

The IEC wind categories I, II, and III in the turbulence intensity of A, B, and C at onshore and offshore conditions are studied. Simulations with different numbers of samples were performed. ~~the~~ The result of the ~~Pf~~ P_f in IEC class I is depicted in Fig. 7.

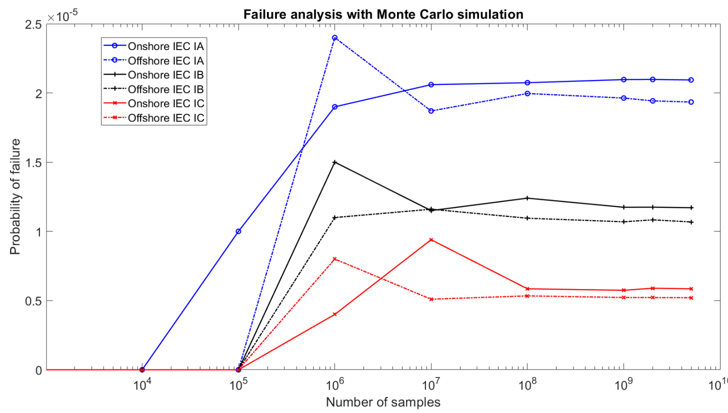

Figure 7. ULS probability of failure of IEC class I wind conditions in different sample numbers in Monte Carlo simulation

As the results show, the ~~Pf~~ P_f converges after 10^7 samples in all wind conditions. To account for a wide range of samples, 10^8 samples were considered in the simulation with the Monte Carlo method, which was repeated 20 times (20 clusters of 10^8 samples). The ~~Pf~~ P_f is the average of 20 clusters. The IEC wind condition probability of failure is illustrated in Fig. 8.

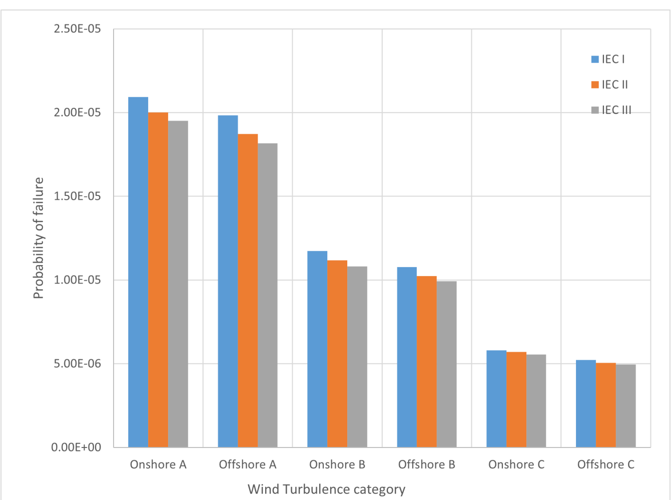

Figure 8. ULS annual probability of failure of IEC wind conditions

IEC onshore A class IA has ~~a reliability of 0.999979, which is the lowest,~~ the highest probability of failure, and the overall probabilities of failures of IEC wind configurations are in the order of 10^{-5}. By increasing the annual mean wind speed, reliability decreases; however, the turbulence intensity has a more significant effect, and reliability decreases when the turbulence intensity increases. While the ~~Pf~~ P_f mean value varies between 2.09×10^{-5} and 4.95×10^{-6}, the standard deviation of the clusters varies between 5.56×10^{-7} and 1.9×10^{-7}. The variance of the results is too small, and it indicates that the clusters are closer together, suggesting less diversity and more consistency. (IEC 61400-1, 2019; IEC 61400-8, 2024) set a target value for the nominal failure probability for structural design for extreme and fatigue failure modes for a reference period of one year is 5×10^{-4} for component class 2. Component class 2 is "safe-life" structural components whose failure may lead to the failure of a major part of a wind turbine, as given in (IEC 61400-8, 2024). All the wind configurations have a lower failure probability than the target value.

~~?~~ (IEC 61400-1, 2019) recommends 15 seed numbers in the ultimate analysis. It is shown that 15 seed numbers cannot represent the behavior of the probability distribution of the extreme loads. To investigate further, the load index is introduced. The load index is the ratio of the extreme ball loads in 300 seed numbers to the extreme ball loads in 15 seed numbers. The load index results ~~of~~ for the IEC wind categories are plotted in Fig. 9. The results show that the extreme load calculation with 15 seeds has an error between 2% and 11%.

This exercise is referred to as a code–site comparison.

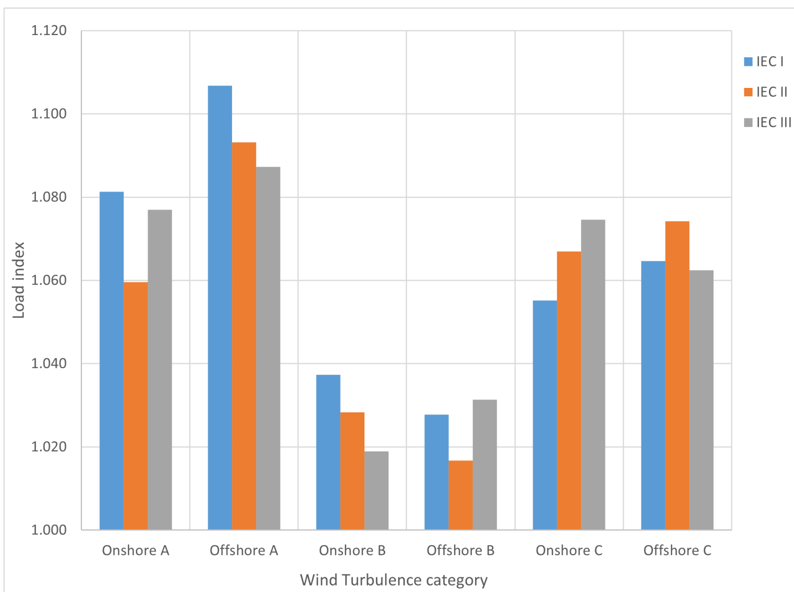

Figure 9. Load index of IEC wind conditions

4.4 Wind sites

The wind sites that were introduced previously were studied. The ~~nominated wind site probability of failures~~ annual probability of failure for the nominated wind sites is illustrated in Fig. 10. ~~To compare the results with the IEC wind condition~~For comparison, the maximum ~~of the Pf in the IEC wind condition is added to~~ P_f value among the IEC wind conditions is also included in the figure.

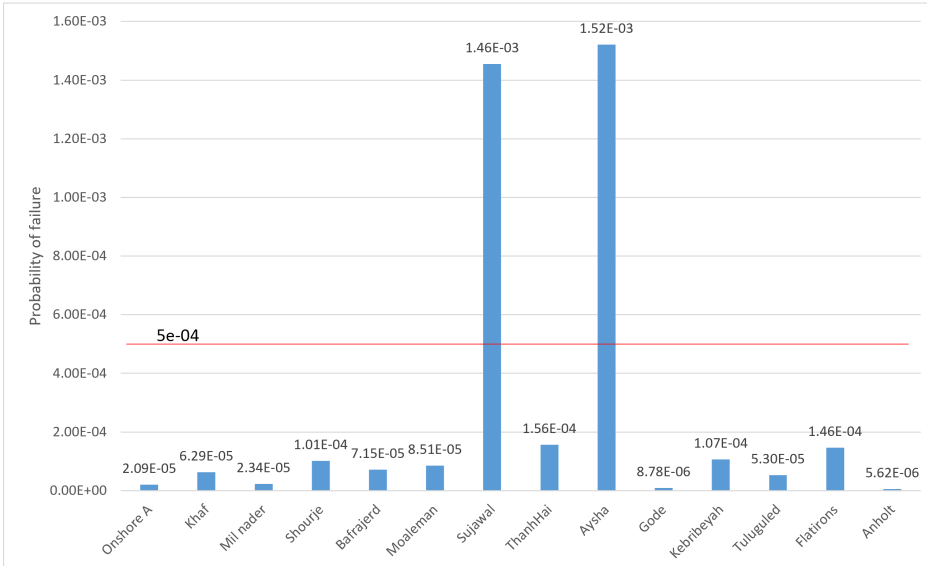

Figure 10. ULS annual probability of failure of nominated wind sites

The results show that most wind sites ~~have~~ exhibit a higher probability of failure in ~~ULS in~~ the blade bearing ~~than the IECs~~under ULS conditions than the IEC categories. The reliability at the Sujawal and Aysha wind sites is far lower than that of the ~~IEC.~~ IECs. In addition, these two sites have higher failure probabilities than the failure target value for component class 2 as given in (IEC 61400-8, 2024). The standard deviation of the clusters varies between 4.82×10^{-6} and 2.33×10^{-7}, and the results of the clusters are consistent. These two wind sites have annual wind speeds between 7.5 and 8.5 and are categorized in the IEC II class, while their ~~Pf~~ P_f is higher than the IEC I class wind sites. The load index results ~~of~~ for the wind sites are plotted in Fig. 11.

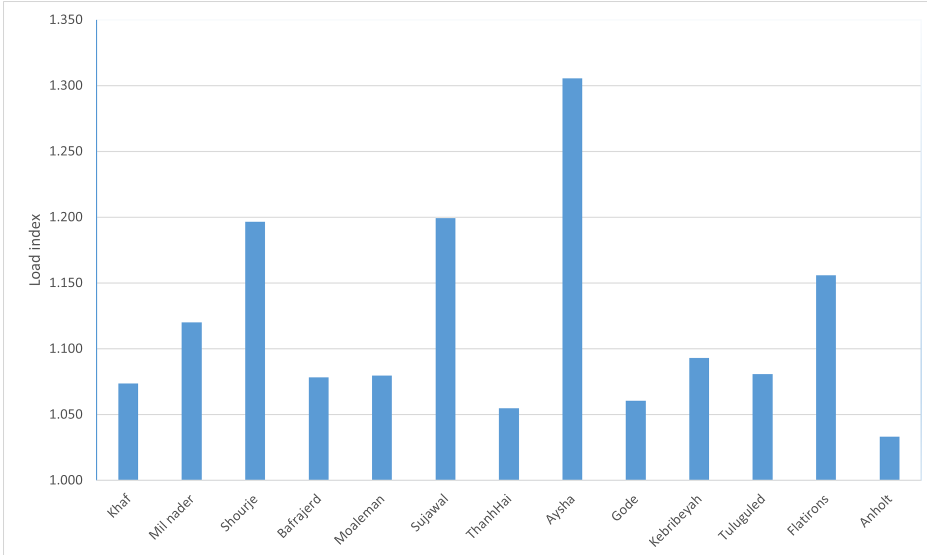

Figure 11. Load index of wind sites

The results show that the extreme load calculation with 15 seeds has an error between 3% and 30%. This observation has important implications for reliability analysis and simulation practice. It shows that using only 15 seeds, as typically done in standard simulations, can lead to a non-negligible underestimation of extreme ball loads, especially in complex wind site conditions. The load index provides a simple and effective measure to quantify this underestimation. It can help practitioners evaluate whether their simulation setup sufficiently captures the load extremes, and when limited seed numbers are used, the load index can offer a basis for applying correction factors to improve the accuracy of failure probability estimates. Additionally, the variation in load index across different wind sites emphasizes the need for site-specific assessment when evaluating blade bearing reliability.

5 Conclusions

The presented work studies the static-overload probability of failure in the double-row, four-point contact ball blade bearing at the ultimate limit state. The static safety factor, which is the ratio between the maximum permissible Hertzian contact stress and the maximum contact stress, is considered for calculating the probability of failure. The NREL 5 MW reference wind turbine is considered with the extreme turbulence wind model in the design load case. The Monte Carlo method was used to calculate the probability of failure. It is shown that the generalized extreme value is a suitable ~~function~~ distribution to simulate the probability of the extreme ball load distribution. ~~By increasing~~ Increasing the number of seeds in ~~simulating the turbulence model,~~ the turbulence simulation improves the accuracy of the ~~probability function increased~~estimated probability distribution. It is observed that by considering 15 seed numbers, as proposed in the standards and guidelines, the ~~effect of different turbulence conditions cannot be achieved~~distribution of the loads is not represented.

The probability of failures of the blade bearing regarding variations of four main dimensions was studied. ~~Ball diameter and raceway~~ Raceway conformity in this aspect ~~have~~ has the highest contribution to the reliability of the blade bearing, and ball diameter is next, and strictly controlling these parameters can lead to higher reliability in the bearing regarding the ultimate limit state.

The ~~pf~~ P_f results of different IEC wind conditions show that the IEC IA onshore category has the highest probability of failure, and the IEC IIIA offshore category has the lowest. However, the ~~effect of~~ wind class (I, II, III)~~and onshore and offshoreis not considerable in~~ , whether onshore or offshore, has minimal impact on the probability of failure~~;~~ , while turbulence intensity (A, B, C) has a significant effect on ~~the~~ reliability. The ~~probability~~ probabilities of failure for the selected onshore and offshore wind sites are ~~mostly worse~~ generally higher than those of IEC sites~~, which indicates that IEC designed~~ . This indicates that IEC-designed turbines may result in lower blade bearing reliability ~~and shorter life if are~~ if used in those wind sites. It also shows the necessity of assessing the blade bearing in every wind site condition according to extreme turbulence wind.

Code and data availability. The code and data used in this study is available upon reasonable request.

Author contributions. AR wrote the original draft. ARN contributed to paper revisions, funding acquisition.

Competing interests. ARN is a member of the editorial board of the Wind Energy Science journal. The authors declare that they have no further conflicts of interest.

Acknowledgements. This research was partially supported by Made4Wind project Under Horizon Europe Research and innovation funding programme under GA No. 101136096.

References

Alavi, O., Mohammadi, K., and Mostafaeipour, A.: Evaluating the suitability of wind speed probability distribution models: A case of study of east and southeast parts of Iran, Energy Conversion and Management, 119, 101–108, https://doi.org/10.1016/j.enconman.2016.04.039, 2016.

Andreasen, D. K., Rodenas-Soler, C., Oertel, U., Krugel, K., Reinares, I., Mendia, I. S., Nielsen, J. H., Olsen, A., Tinni, A., Vizireanu, D., Cheaytani, J., Kratz, M., and Bousseau, P.: Portability of failure mode detection/prognosis orientations 2.0, Tech. rep., ROMEO, https://www.romeoproject.eu/wp-content/uploads/2022/10/D2_4_Portability_2_3_final.pdf, 2022.

Bain, L. J. and Antle, C. E.: Estimation of Parameters in the Weibull Distribution, Technometrics, 9, 621–627, 1967.

Cheng, H., Zhang, Y., Lu, W., and Yang, Z.: Reliability sensitivity analysis based on stress–strength model of bearing with random parameters, Review of Scientific Instruments, 91, 073 908, https://doi.org/10.1063/1.5143405, 2020.

Daidié, A., Chaib, Z., and Ghosn, A.: 3D Simplified Finite Elements Analysis of Load and Contact Angle in a Slewing Ball Bearing, Journal of Mechanical Design, 130, 082 601, https://doi.org/10.1115/1.2918915, 2008.

Dawson, C., Abrahart, R., and See, L.: HydroTest: a web-based toolbox of evaluation metrics for the standardised assessment of hydrological forecasts, Environmental Modelling & Software, 22, 1034–1052, https://doi.org/10.1016/j.envsoft.2006.06.008, 2007.

Ditlevsen, O. and Madsen, H.: Structural Reliability Methods, Technical University of Denmark, https://books.google.no/books?id=Z1LOPwAACAAJ, 2007.

DNV-ST-0437: Loads and site conditions for wind turbines, 2016.

Germanischer Lloyd: Guideline for the Certification of Wind Turbines, 2010.

GIZ: Vietnam - Wind Measurement Data, https://energydata.info/dataset/vietnam-wind-measurements-giz, [Online; accessed 20-January-2023], 2023.

Graßmann, M., Schleich, F., and Stammler, M.: Validation of a finite-element model of a wind turbine blade bearing, Finite Elements in Analysis and Design, 221, 103 957, https://doi.org/https://doi.org/10.1016/j.finel.2023.103957, 2023.

Harris, T., Rumbarger, J., and Butterfield, C.: Wind Turbine Design Guideline DG03: Yaw and Pitch Rolling Bearing Life, Tech. rep., NREL/TP-500-42362, National Renewable Energy Lab.(NREL), Golden, CO (United States), https://doi.org/10.2172/969722, 2009.

Harris, T. A. and Kotzalas, M. N.: Rolling bearing analysis-2 volume set, Crc Press, 2006.

Haus, L., Sheng, S., and Pulikollu, R. V.: Wind Turbine Major Systems Reliability Trends and Mitigation Strategies, https://app.box.com/s/ktjzjdxn77omu1cjoy9znymbrynlsw0d.

IEA: Renewable Energy Market Update Outlook for 2023 and 2024, Tech. rep., International Energy Agency (IEA), https://www.iea.org/reports/renewable-energy-market-update-june-2023, 2023.

IEC 61400-1: Wind energy generation system, part 1: Design requirements, https://webstore.iec.ch/publication/26423, 2019.

IEC 61400-3-1: Wind energy generation systems - Part 3-1: Design requirements for fixed offshore wind turbines, https://webstore.iec.ch/en/publication/29360, 2019.

IEC 61400-3-2: Wind energy generation system, Part 3-2: Design requirements for floating offshore wind turbines, https://webstore.iec.ch/en/publication/29244, 2019.

IEC 61400-8: Wind energy generation system, Part 8: Design of wind turbine structural components, https://webstore.iec.ch/en/publication/61824, 2024.

Imdad, A., Arniella, V., Zafra, A., and Belzunce, J.: Tensile behaviour of 42CrMo4 steel submitted to annealed, normalized, and quench and tempering heat treatments with in-situ hydrogen charging, International Journal of Hydrogen Energy, 50, 270–280, https://doi.org/https://doi.org/10.1016/j.ijhydene.2023.10.082, 2024.

ISO 19902: Petroleum and natural gas industries — Fixed steel offshore structures, https://www.iso.org/standard/65688.html, 2020.

ISO 19904-1: Petroleum and natural gas industries — Floating offshore structures, Part 1: Ship-shaped, semi-submersible, spar and shallow-draught cylindrical structures, https://www.iso.org/standard/63801.html, 2019.

ISO 2394: General principles on reliability for structures, https://www.iso.org/standard/58036.html, 2015.

ISO 2768-1: General tolerances- Part 1: Tolerances for linear and angular dimensions without individual tolerance indications, ISO, https://www.iso.org/standard/7748.html, 1989.

ISO 76: Rolling bearings — Static load ratings, https://www.iso.org/standard/38101.html, 2006.

Jager, D. and Andreas, A.: NREL National Wind Technology Center (NWTC): M2 Tower; Boulder, Colorado (Data);, Tech. rep., NREL Report No. DA-5500-56489, https://doi.org/10.5439/1052222, 1996.

Jonkman, B.: TurbSim User's Guide: Version 1.50, Tech. rep., NREL/TP-500-46198, National Renewable Energy Lab.(NREL), Golden, CO (United States), https://doi.org/10.2172/965520, 2009.

Jonkman, J., Butterfield, S., Musial, W., and Scott, G.: Definition of a 5-MW reference wind turbine for offshore system development, Tech. rep., National Renewable Energy Lab.(NREL), Golden, CO (United States), https://doi.org/10.2172/947422, 2009.

Keller, J. and Guo, Y.: Rating of a Pitch Bearing for a 1.5-MW Wind Turbine, Tech. rep., NREL/TP-5000-82462, National Renewable Energy Lab.(NREL), Golden, CO (United States), https://doi.org/10.2172/1902646, 2022.

Lai, J.: A new model for the static load rating of surface induction-hardened bearings, Evolution, 2, 27–32, 2011.

Lai, J., Ovize, P., Kuijpers, H., Bacchettto, A., and Ioannides, S.: Case Depth and Static Capacity of Surface Induction-Hardened Rings, Journal of ASTM International, 6, 1–16, https://doi.org/10.1520/JAI102630, 2009.

Leupold, S., Schelenz, R., and Jacobs, G.: Method to determine the local load cycles of a blade bearing using flexible multi-body simulation, Forsch. Ingenieurwes, 85, 211–218, https://doi.org/https://doi.org/10.1007/s10010-021-00457-y, 2021.

Lewis, S., Gaillard, L., Seiler, R., Parzianello, G., and LeLetty, R.: Recent Steps Towards a Common Understanding of Ball Bearing Load Capacity, in: ESA Special Publication, edited by Ouwehand, L., vol. 737 of *ESA Special Publication*, p. 35, 2015.

Melchers, R. E. and Beck, A. T.: Structural reliability analysis and prediction, John wiley & sons, 2018.

Menck, O., Stammler, M., and Schleich, F.: Fatigue lifetime calculation of wind turbine blade bearings considering blade-dependent load distribution, Wind Energy Science, 5, 1743–1754, https://doi.org/10.5194/wes-5-1743-2020, 2020.

Mishnaevsky Jr, L. and Thomsen, K.: Costs of repair of wind turbine blades: Influence of technology aspects, Wind Energy, 23, 2247–2255, 2020.

Nejad, A. R.: Modelling and analysis of drivetrains in offshore wind turbines, Offshore wind energy technology, 37, 2018.

Rezaei, A. and Nejad, A. R.: Effect of wind speed distribution and site assessment on pitch bearing loads and life, Journal of Physics: Conference Series, 2507, 012 021, https://doi.org/10.1088/1742-6596/2507/1/012021, 2023.

Rezaei, A., Guo, Y., Keller, J., and Nejad, A. R.: Effects of wind field characteristics on pitch bearing reliability: a case study of 5 MW reference wind turbine at onshore and offshore sites, Forschung im Ingenieurwesen, 87, 321–338, 2023.

Rezaei, A., Schleich, F., Menck, O., Grassmann, M., Bartschat, A., and Nejad, A. R.: Comparative analysis of rolling contact fatigue life in a wind turbine pitch bearing with different modeling approaches, in: Journal of Physics: Conference Series, vol. 2767, p. 052036, IOP Publishing, 2024.

SATBA, R.: http://www.satba.gov.ir/en/, [Online; accessed 24-May-2022], 2022.

Schwack, F., Stammler, M., Poll, G., and Reuter, A.: Comparison of life calculations for oscillating bearings considering individual pitch control in wind turbines, in: Journal of Physics: Conference Series, vol. 753, p. 112013, IOP Publishing, 2016.

Shi, H., Z. Dong, N. X., and Huang, Q.: Wind Speed Distributions Used in Wind Energy Assessment: A Review, Frontiers in Energy Research, 9, 769 920, 2021.

Shimizu, S., Tosha, K., and Tsuchiya, K.: New data analysis of probabilistic stress-life (P–S–N) curve and its application for structural materials, International Journal of Fatigue, 32, 565–575, https://doi.org/10.1016/j.ijfatigue.2009.07.017, 2010.

Stammler, M., Menck, O., Guo, Y., and Keller, J.: Wind Turbine Design Guideline DG03: Yaw and Pitch Bearings, Tech. rep., NREL/TP-5000-89161, National Renewable Energy Lab.(NREL), Golden, CO (United States), https://doi.org/https://doi.org/10.2172/2406870, 2024.

Stehly, T., Duffy, P., and Hernando, D. M.: Cost of Wind Energy Review: 2024 Edition, Tech. rep., NREL/PR-5000-91775, National Renewable Energy Lab.(NREL), Golden, CO (United States), https://doi.org/10.2172/2479271, 2024.

Wang, X. and Zhang, T.: Plastic deformation-based rolling bearing reliability and sensitivity analysis under incomplete probability information, Advances in Mechanical Engineering, 14, 16878132221142 968, https://doi.org/10.1177/16878132221142968, 2022.

Wang, X., Wang, B., Chang, M., and Li, L.: Reliability and sensitivity analysis for bearings considering the correlation of multiple failure modes by mixed Copula function, Proceedings of the Institution of Mechanical Engineers, Part O: Journal of Risk and Reliability, 234, 15–26, https://doi.org/10.1177/1748006X19876137, 2020.

Wang, Y., Wang, W., and Zhao, Z.: Effect of race conformities in angular contact ball bearing, Tribology International, 104, 109–120, https://doi.org/10.1016/j.triboint.2016.08.034, 2016.

World Bank Group: Ethiopia - Wind Measurement Data, https://energydata.info/dataset/ethiopia-wind-measurement-data, [Online; accessed 20-January-2023], 2023a.

World Bank Group: Pakistan - Wind Measurement Data, https://energydata.info/dataset/pakistan-wind-measurement-data, [Online; accessed 20-January-2023], 2023b.

Yu, J., Fu, Y., Yu, Y., Wu, S., Wu, Y., You, M., Guo, S., and Li, M.: Assessment of Offshore Wind Characteristics and Wind Energy Potential in Bohai Bay, China, Energies, 12, https://doi.org/10.3390/en12152879, 2019.

Ørsted: Green solutions: Offshore wind data, https://orsted.com/en/our-business/offshore-wind/wind-data, [Online; accessed 4-June-2022], 2022.